

## HiSST: 4th International Conference on High-Speed Vehicle Science Technology 22 -26 September 2025, Tours, France



# Experimental verification of PIV-based aerodynamic load reconstruction measurement method for supersonic nozzle

Jie Tian, Kunyuan Zhang, Jinglei Xu

#### **Abstract**

Conventional balance force measurement systems are limited to measuring the overall loads and cannot decouple individual component contributions, which restricts the exploration of the flow mechanism behind aerodynamic loads. With the advancement of Particle Image Velocimetry (PIV) technology, a PIV-based aerodynamic load measurement technique has been proposed, which indirectly measures aerodynamic loads by reconstructing multiple physical fields such as pressure and density. However, the performance of conventional pressure field reconstruction methods is severely reduced when applied to supersonic flow fields, which limits the extension of PIV-based aerodynamic load reconstruction method to supersonic nozzles. To address these challenges, this study proposes a supersonic pressure field reconstruction method for supersonic flow and a thrust performance reconstruction measurement for supersonic nozzle based on Flow Vector Splitting (FVS) technology. Through PIV experiments conducted in a direct-connect nozzle wind tunnel, we reconstructed multiphysics fields and aerodynamic performance parameters (including mass flow rate, thrust, and lift) under typical operating conditions. Evaluation results show that the reconstructed data calculated based on FVS method achieves higher accuracy and better self-consistency, satisfying conservation laws of mass flow and momentum. The relative errors of thrust and lift under over expansion conditions are merely -1.70% and 0.60%, respectively. The local errors in post-shock wall pressure remain below 3%. These results outperform conventional Poisson method and spatial integration method. Therefore, the experimental results have verified the feasibility and high accuracy of the PIV-based thrust performance reconstruction methodology for supersonic nozzles, which can provide valuable complementary data to conventional balance force measurement technology.

## Keywords: Particle Image Velocimetry (PIV), pressure reconstruction, aerodynamic load measurement, Flow Vector Splitting (FVS)

#### **Nomenclature**

*e* – internal energy

**F**- conservative fluxes in x direction

**G** – conservative fluxes in y direction

J – viscous terms

 $\dot{m}$  – mass flow rate

*p* – pressure

*T* – temperature

Th – thrust

**U** – conservative primitive variables

u – velocity in x direction

 $\nu$  – velocity in y direction

Greek

 $\rho$  – density

 $\gamma$ -specific heat ratio

Superscripts

t – time

Subscripts

i –parameter in x direction j –parameter in y direction



## HiSST: 4th International Conference on High-Speed Vehicle Science Technology 22 -26 September 2025, Tours, France



#### 1. Introduction

The nozzle is the core component that generates thrust in aircraft engine. When conducting wind tunnel experiments on nozzles for performance testing, the main focus is on evaluating the basic aerodynamic performance, including thrust coefficient and discharge coefficient, by measuring flow rate, as well as aerodynamic loads such as thrust, lift, and pitch moment. As a consequence, the aerodynamic load measurement system is the most critical measurement system in wind tunnel experiments for aircraft exhaust systems. What is more, the six-component force balance currently represents the most standardized and mature wind tunnel force measurement equipment, characterized by advantages of high accuracy, precision, and resolution [1][2].

However, the measurement principle of balances resembles a "black box" physical model, where measured values reflect the coupled effects of integrated loads acting on the model. This imposes inherent limitations. First, balances cannot decouple individual components' contributions to overall aerodynamic loads. Taking the Over-Under Turbine-Based Combined-Cycle (TBCC) engine nozzle as an example, when operating under combined ramjet and turbine modes, the balance cannot separate thrust performance parameters of each channel or evaluate dual-channel coupling effects [3]. Second, balances cannot decompose the proportional contributions of aerodynamic parameter components to total loads, which means that it remains impossible to quantify the values and proportions of inlet/outlet momentum, pressure differential forces, or wall forces. In summary, as a "black box" model, balances cannot correlate aerodynamic loads with flow field parameters or structures, severely restricting exploration of flow mechanisms underlying aerodynamic loads. Additionally, coupled balance measurement systems significantly increase the complexity and cost of wind tunnel design, while their contact-based measurement nature creates challenges in simultaneously achieving optimal force transmission and sealing performance during design and installation.

Under the engineering requirements, developing new measurement technologies has emerged as a crucial research direction, which aim to synchronously measure the aerodynamic parameters/loads in exhaust systems, establish tight correlations between load distributions and flow field structures, and decouple component/parameter contributions to integrated loads. Early indirect measurement methods-including wake survey and contour integration method which have been widely used for aerofoil drag measurement—are fundamentally control volume methods based on momentum conservation [4]. However, early velocity measurement techniques could only estimate momentum and pressure terms through wake rakes or pitot-static probes combined with Bernoulli equations, restricting the applications within low Mach number flows. Particle Image Velocimetry (PIV) has matured as a reliable, high-accuracy/precision, high-resolution measurement technology to obtain full-field and instantaneous velocity quantitatively [5][6]. Its capabilities perfectly align with control volume method requirements, evolving into PIV-based aerodynamic load measurement technology that has been successfully applied to lift/drag measurements in subsonic/transonic airfoil flows [7]-[10]. The procedure involves: 1) Acquiring high-quality velocity fields via PIV; 2) Reconstructing multi-physical fields, such as pressure, temperature and density based on Navier-Stokes (N-S) equations; 3) Implementing control volume analysis for indirect aerodynamic load measurement.

Despite maturity in subsonic/transonic external flows, PIV-based load reconstruction measurement method has not been effectively extended to supersonic internal flows in engine components, such as nozzles, inlets and cascades [11][12]. This stems from two key limitations: 1) Significant challenges in PIV measurements for supersonic internal flows—exemplified by overexpanded ramjet nozzles which containing complex phenomena like shock intersections, shock/boundary layer interactions, and large-scale separations—compromise velocity field accuracy; 2) This method requires high-accuracy pressure field reconstruction, yet conventional techniques face fundamental limitations in supersonic flows. Poisson method's elliptic governing equations are in conflict with the supersonic flow principle where downstream cannot influence upstream, while Spatial Integration (SI) method fail to handle parameter

discontinuities at shocks. As a result, both of them face critical accuracy degradation post-shock [13][14].

To address these challenges, this study proposes a supersonic pressure field reconstruction method based on Flux Vector Splitting (FVS) technique to improve the accuracy of reconstructed multi-physical fields and further optimizes the PIV-based aerodynamic load measurements in supersonic nozzles. A direct-connect wind tunnel test bench was constructed for PIV velocity field measurements. Experimental investigations focus on supersonic internal flows of the two-dimensional nozzle models, one is Single Expansion Ramp Nozzle (SERN) under typical operating conditions and the other is the Wind Tunnel Nozzle (WTN) with the designed Mach number of 2.5. Subsequently, multi-physical fields are reconstructed and the reconstruction accuracy can be evaluated against the static pressure probe measurements. Control volumes were further established to calculate nozzles' performance parameters with accuracy assessments.

#### 2. Basic principles and procedures

## 2.1. Principle of PIV-based FVS method

Establishing high-accuracy pressure field reconstruction methods is a prerequisite for implementing PIV-based non-contact load measurement technology. The essence of this approach lies in inversely solving the N-S equations using PIV velocity data. However, conventional reconstruction approaches are unsuitable for supersonic flow fields in principle. In numerical simulations, mathematical discontinuities in supersonic flows originate from the inviscid terms of the equations [15]. Given that appropriate difference discretization schemes can reduce numerical errors, the FVS method is proposed. This method processes the conservative form of the N-S equations through flux vector splitting, constructs difference schemes based on the characteristic propagation directions of physical waves, and thus, combines the advantages of conforming to supersonic physical characteristics and reducing numerical discretization errors. This chapter explains the principles, including governing equations, boundary conditions, the finite difference scheme, and the iterative process.

For two-dimensional compressible flows, the conservative momentum equation in the mainstream direction and energy equation are selected as the basic equations. Thus, four unknown variables exist: density  $\rho$ , pressure p, temperature T, and internal energy e. To close the control equations, the gas state equation and the calorimeter state equation are introduced. The matrix form of the equations is expressed as follows:

$$\frac{\partial U}{\partial t} = J - \frac{\partial F}{\partial x} - \frac{\partial G}{\partial y} \tag{1}$$

where  $\boldsymbol{U}$  denotes conservative primitive variables,  $\boldsymbol{F}$  and  $\boldsymbol{G}$  denote conservative fluxes of momentum and energy, **J** denotes viscous terms.

Considering that the N-S equations exhibit complex elliptic-parabolic mathematical characteristics, a time derivative term is introduced in Eq. (1) to formulate a well-posed problem for time-marching solutions. Furthermore, under the adiabatic assumption, the energy equation can be replaced by Eq. (2):

$$T = T_{\infty} \left( 1 + \frac{\gamma - 1}{2} M_{\infty}^2 \left( 1 - \frac{V^2}{V_{\infty}^2} \right) \right)$$
 (2)

Additionally, appropriate boundary conditions and initial conditions must be specified. The core iterative variable in the FVS method is density and the Neumann boundary condition for density is directly applied (Eq. (3)). Notably, this formulation does not rely on isentropic assumptions, making it applicable to boundaries involving non-isentropic flows with shocks. The initial multi-physical fields are assigned using the isentropic method.

$$\rho = \rho_{\infty} \left( 1 + \frac{\gamma - 1}{2} M_{\infty}^2 \left( 1 - \frac{V^2}{V_{\infty}^2} \right) \right)^{\frac{1}{\gamma - 1}}$$
(3)

The key advantage of the FVS method in handling supersonic flows with complex wave systems lies in its flux vector splitting scheme and finite difference scheme, which align with supersonic flow physics. First, the Jacobian coefficient matrix of the equations is split into eigenvalues, and the flux vectors F

and **G** are decomposed into positive and negative components based on these eigenvalues [16][17]. This study employs the classical Steger-Warming splitting method, where flux splitting strictly follows the characteristic directions of physical waves. Second, upwind difference scheme is adopted for spatial derivatives: backward difference scheme for positive fluxes and forward difference scheme for negative fluxes. This approach ensures that parameter calculations follow characteristic wave propagation and depend on upstream information, adhering to supersonic flow physics. Compared to the central differencing operators used in traditional Poisson methods, these one-sided operators better handle discontinuities at shocks. Finally, assuming density and temperature are known at time level t, and then parameters at  $t+\Delta t$  are solved through the following time-marching iterative expression:

$$U_{i,j}^{t+\Delta t} = U_{i,j}^{t} + \Delta t \left[ J_{i,j}^{t} - \left( \frac{\left( F^{+} \right)_{i,j}^{t} - \left( F^{+} \right)_{i-1,j}^{t}}{\Delta x} + \frac{\left( F^{-} \right)_{i+1,j}^{t} - \left( F^{-} \right)_{i,j}^{t}}{\Delta x} \right) - \left( \frac{\left( G^{+} \right)_{i,j}^{t} - \left( G^{+} \right)_{i,j-1}^{t}}{\Delta y} + \frac{\left( G^{-} \right)_{i,j+1}^{t} - \left( G^{-} \right)_{i,j}^{t}}{\Delta y} \right) \right]$$
(4)

### 2.2. Principle of PIV-based load reconstruction method

Given that the FVS method enables reconstruction of multi-physical fields including pressure, temperature, and density, this allows further development of reconstruction measurement methods for nozzle performance parameters such as thrust and lift.

First, calculate the mass flow rate  $\dot{m}$  at the nozzle's inlet/outlet sections. The area integration in the flow rate formula is discretized using the trapezoidal rule. Subsequently, compute the nozzle gross thrust *Th*, defined as the axial residual impulse at the nozzle exit:

$$Th = \dot{m}u_e + (p_e - p_a)A_{ex} \tag{5}$$

where subscript e denotes the nozzle exit and x represents the axial direction.

For the nozzle control volume, the momentum theorem further expresses gross thrust T using aerodynamic parameters at the inlet:

$$Th = \dot{m}u_{in} + (p_{in} - p_a)A_{in,x} - R_x$$
 (6)

where subscript in denotes inlet parameters, and R<sub>x</sub> represents the axial projection of the aerodynamic force exerted by the gas on the nozzle control volume. This indicates that nozzle thrust can be calculated from inlet momentum flux and aerodynamic loads on the nozzle walls. Pressure and momentum terms are similarly discretized using the trapezoidal rule for numerical solutions.

The reconstructed thrust results from these two calculation methods can be compared and evaluated. The relative error  $E_T$  is calculated using Eq. (7) as the reference. Constrained by momentum conservation law, the two thrust formulas should theoretically yield equal values. Thus, Er reflects selfconsistency of the experimental and reconstructed data (i.e., deviation from momentum conservation laws) and indirectly validates measurement accuracy.

$$E_{T} = \frac{\left(\dot{m}_{e}u_{e} + p_{e}A_{ex}\right) - \left(\dot{m}_{in}u_{in} + p_{in}A_{in,x} - R_{x}\right)}{\dot{m}_{in}u_{in} + p_{in}A_{in,x} - R_{x}} \times 100\%$$
(7)

## 3. PIV System and Model Calibration

#### 3.1. PIV system

Lavision's low-frequency Flow-Master@Tomo-PIV system was used and the two-dimension twocomponent (2D2C) working mode was selected for measurement. Illumination was provided by a Litron dual-pulse Nd: YAG laser outputting 200 mJ at a wavelength of 532 nm and a repetition frequency of 10 Hz. The laser beam was formed into a 1.5 mm thick sheet. The images were captured by an Imager SX 6M, with a CCD resolution of  $2752 \times 2200$  pixels, equipped with a Zeiss fixed-focus lens of 50 mm. Diethyl-hexyl-sebacat (DEHS) droplets, of approximately 0.5-1 µm nominal particle diameter, were generated and injected through the seeding rake.

#### 3.2. SERN model

The two-dimensional SERN model is shown in Fig. 1. The model features a contraction section inlet height of 0.04 m, a throat height of 0.02 m, and an expansion section exit height of 0.1 m. The convergent profile is designed using the Vitoshinsky formula, with a large throat curvature radius implemented to approximate the sonic line at the throat as a straight line perpendicular to the horizontal lip. To facilitate wall masking during PIV experiments, the expansion surface downstream of the throat profile adopts a constant-slope straight line. The PIV field of view (FOV) and real-time calibration images of the model are displayed in Fig. 2. FOV size is  $103.8 \times 82.78 \text{ mm}^2$ , with a raw particle image magnification of 37.63 µm/pixel and digital magnification ratio of 26.57 pixel/mm. Given the maximum local velocity slightly exceeding 600 m/s in this experiment, tracer particle displacements between frames A and B are approximately 0.5 mm, corresponding to 13 pixels. Following the 1/4 rule, the interrogation window sizes for WiDIM cross-correlation processing are set as 64 × 64 pixels<sup>2</sup> for the initial pass and  $32 \times 32$  pixels<sup>2</sup> for the final iteration, with an overlap factor of 75%. This configuration yields adjacent velocity vector spacing of 0.30 mm, corresponding to the final spatial resolution.

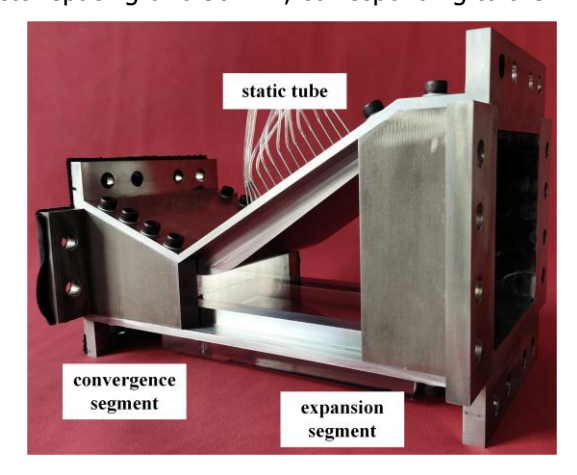


Fig 1. Experimental model of SERN

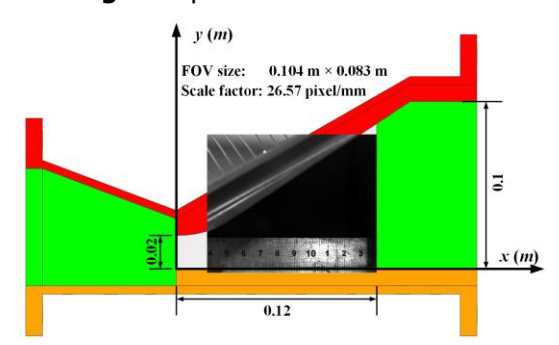


Fig 2. Real-time calibration image of FOV of SERN

## 3.3. WTN model

Two-dimensional WTN is shown in Fig. 3. The convergent profile adopts the Witoszynski curve, assuming a uniform sonic inflow at the throat. The expansion profile is designed using the Busemann method. The nozzle exit is designed with a Mach number of 2.5. To capture the complete diamondshaped region upstream of the nozzle exit, both left and right walls of the expansion section are integrated with optical windows. The upper wall features a high-transparency PMMA to minimize surface reflection noise and enhance near-wall PIV measurements, while the lower wall consists of a metal surface with optical windows for laser sheet illumination. The PIV field of view (FOV) and real-time calibration images of the model are displayed in **Fig. 4**. FOV size is 144 × 115 mm<sup>2</sup>, with a raw particle image magnification of 52.32 µm/pixel and digital magnification ratio of 19.11 pixel/mm. Similarly, the adjacent velocity vector spacing is calculated as approximately 0.42 mm, corresponding to the final spatial resolution.



Fig 3. Experimental model of WTN

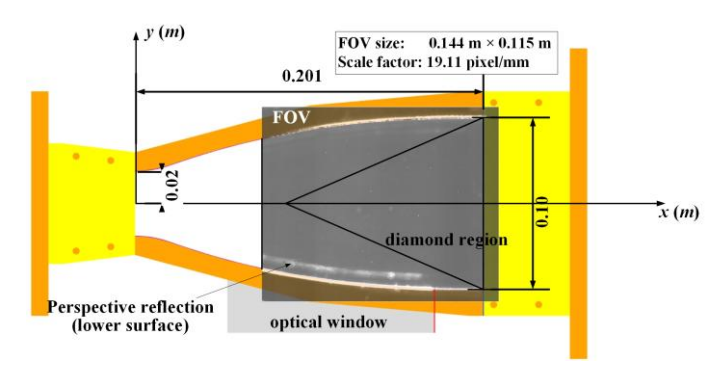


Fig 4. Sketch of calibration image of WTN

#### 3.4. Direct-connect wind tunnel test

Ground-based wind tunnel test benches are generally categorized into direct-connect and free-jet configurations. The direct-connect wind tunnel offers advantages including superior starting performance, lower operating costs, and extended operational duration, while the free-jet wind tunnel better simulates external flow environments and external wave structures [18]. For wind tunnel experiments validating nozzle design performance, free-jet mode is typically adopted to study coupled effects between internal and external supersonic flows. However, this experiment aims to validate the feasibility and performance of thrust reconstruction measurement methods, focusing on reconstructing nozzle inlet/outlet flow rates and full-field pressure. For predetermined operating conditions, external flow effects need not be considered. Therefore, the direct-connect test fully satisfies verification requirements while offering higher efficiency.

The direct-connect nozzle test is illustrated in Fig. 5, comprising a transition section, stabilization section, test section, and expansion section, connected via valves to downstream vacuum sphere tanks. The pure suction mode was adopted in these experiments, with upstream atmospheric intake and downstream vacuum suction. Backpressure variation is controlled to switch nozzle operating states. Unlike free-jet nozzle tests, the direct-connect configuration lacks a vacuum chamber to simulate external environmental pressure, eliminating the distinction between nozzle exit pressure and ambient pressure. Consequently, Eq. (5) and (6) are modified to calculate absolute thrust values without considering ambient pressure.

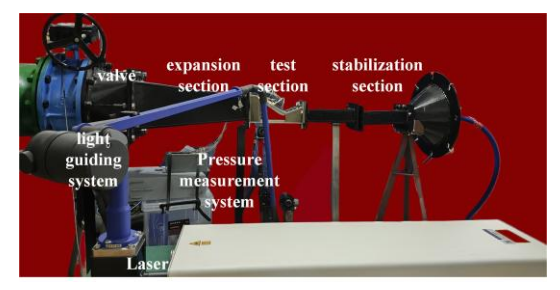


Fig 5. Direct-connect wind tunnel test

#### 4. PIV Velocity Data and Reconstruction Results

Given that PIV raw particle images can visualize flow field structures through grayscale distributions reflecting tracer particle density, they enable real-time assessment of nozzle internal flow states when combined with quantitative time-averaged static pressure  $p_w$  on the upper wall. For the SERN model, the experimental inflow total pressure was 101500 Pa with a total temperature of 290 K. Two typical operating conditions were measured. Case 1 corresponds to the SERN working in the fully-expanded state ( $p_w = 3609 \text{ Pa}$ ); case 2 corresponds to the SERN working in the over-expanded state, featuring oblique shocks within the channel and flow separation along the upper wall ( $p_w = 10174 \text{ Pa}$ ). For the WTN model, experiments were conducted at the fully-expanded condition with inflow total pressure of 101500 Pa and total temperature of 295 K.

For all cases, the measured velocity fields and reconstruction results are presented. Given that the simple direct-connect wind tunnel lacks a balance system and a flow meter, case-by-case evaluations on mass flow rate and aerodynamic load are conducted subsequently. For the SERN model, the FVS method are compared with conventional methods to validate its superior performance. Wall pressure probes, combined with mass conservation and momentum conservation, are all used for comprehensive evaluation. For the WTN model, additional theoretical and simulation evaluation can be available.

Moreover, it is important to note that the FVS method proposed in this paper only involves two-dimensional flows. Therefore, only a two-dimensional, two-component (2D-2C) PIV mode was employed to measure the velocity field on the mid-span plane of the quasi-two-dimensional nozzle models. The reconstructed or simulated flow rate and thrust results are all assumed as the per-unit-spanwise-length quantities.

#### 4.1. Case 1 of SERN

**Fig. 6** presents the velocity field data of SERN within the target field of view (FOV) under Case 1 conditions ( $p_w = 3609 \text{ Pa}$ ). Here, ROI denotes the Region of Interest selected for subsequent multiphysical field reconstruction, corresponding to the area enclosed by the white trapezoidal frame. The ROI boundary spans from x=0.022 m to x=0.108 m. To minimize approximation errors and maximize utilization of the spatial resolution limit of PIV, the control boundary was positioned within 1 mm of the wall. Velocity contour demonstrates the **fully-expanded** working condition. This test case enables simulation of under-expanded, fully expanded, and slightly over-expanded flow conditions of the SERN. **Fig. 7** shows the contours of the velocity fields for the u- and v-velocity components respectively.

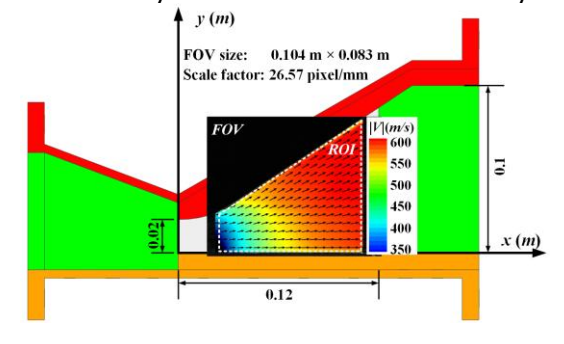


**Fig 6.** Contour of velocity field (case 1 of SERN)

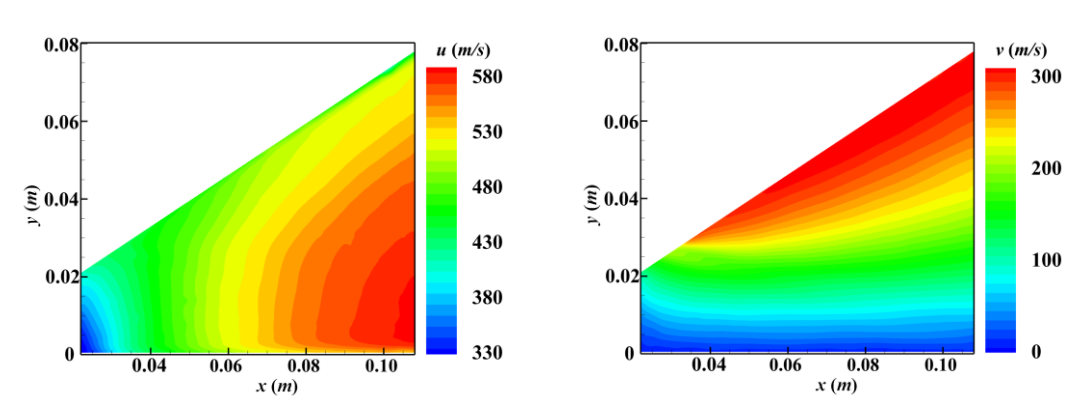


Fig 7. Contours of velocity component (case 1 of SERN)

**Fig. 8(a)~(c)** presents the reconstructed pressure field contours over the aforementioned trapezoidal ROI by different methods. The results were normalized using the inflow total pressure. Performance of the FVS method was evaluated by comparison with the conventional Poisson method and the SI method. Considering that pressure probes suffer limited resolution and would inevitably disturb flow structures, it remains challenging to obtain reasonably full-field reference pressure data quantitatively for evaluating the reconstruction results. Therefore, as a fallback option, the static pressure distributions along the upper wall are measured for evaluation, as shown in **Fig. 8(d)**. Uniformly, the results of Methods A, B, and C are represented in red, green, and blue, respectively. Throughout this paper, pressure results using probe measurements, Poisson method, SI method, and FVS method, are uniformly represented by black, red, green, and blue, respectively.

All three reconstructed pressure fields are similar, indicating great agreement with the probe measurement. Among them, the SI and FVS methods demonstrate relatively higher reconstruction accuracy, with the error level maintained below 3%, while the Poisson method results exhibit a slight overall overestimation. As reviewed previously, both Poisson and SI methods do not suffer from severe degradation in this case, owing to the fully expanded and shock-free nozzle flow.

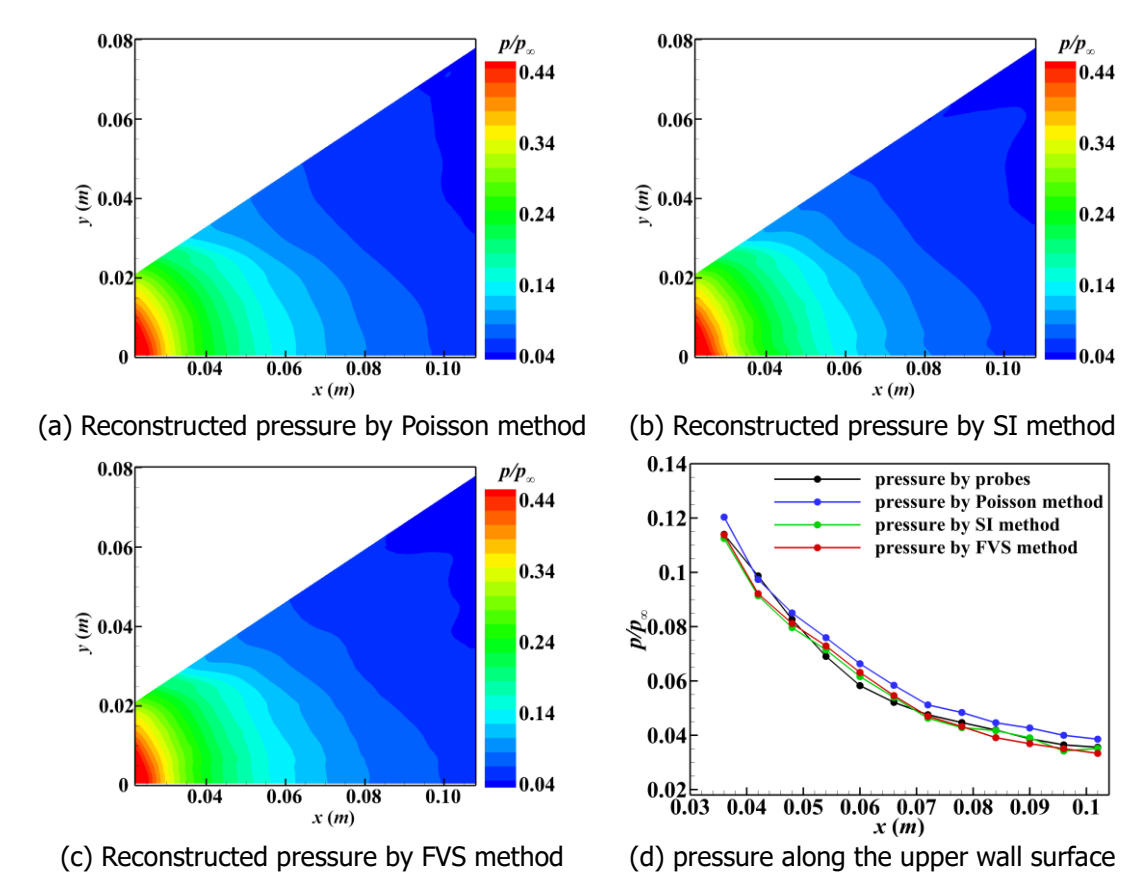


Fig 8. Reconstructed pressure results by different methods (case 1 of SERN)

Utilizing above reconstructed multi-physics field results, key performance parameters such as nozzle flow rate, thrust, and lift can be further derived. First, we evaluate the mass flow rate. **Fig. 9** illustrates the results extracted at successive cross-sections along the nozzle axis. All three datasets exhibit identical trends. The curves, originating from 4.40 kg/s at the upstream initial section, increases sharply to a peak of 4.95 kg/s at x=0.035 m and subsequently stabilizes. This behavior arises because the upper control-volume boundary, corresponding to the throat transition region of x<0.035 m, fails to conform to the upper wall. Thus, only the constant-slope expansion section (x>0.035 m) provides a valid approximation. The results indicate the satisfaction of mass conservation laws, validating the mutual consistency between multi-physics fields—both measured and reconstructed data. Furthermore, the SERN's theoretical isentropic flow rate is calculated as 4.82 kg/s. Given the nozzle's full expansion state and the consequently high discharge coefficient under through-flow conditions, the errors remain controllable within 5% by the FVS method even when accounting for boundary layer displacement losses, demonstrating its comparatively superior accuracy as well.

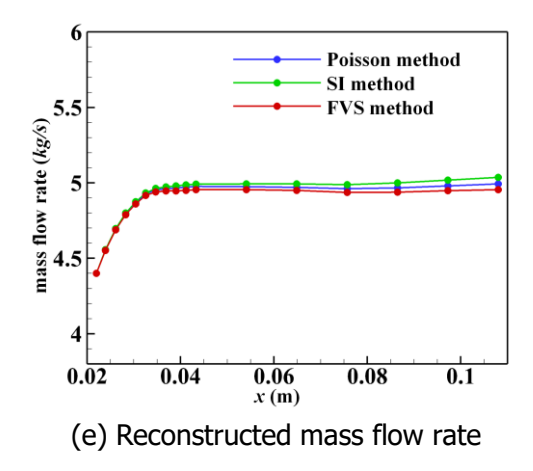


Fig 9. Reconstructed mass flow rate results by different methods (case 1 of SERN)

Section 2.2 introduces two computational approaches for determining gross thrust of nozzle, namely, direct extraction of outlet residual impulse, a combined computation using inlet impulse and wall forces. Before reconstruction, an appropriate control volume satisfying mass conservation was divided first based on ROI, spanning from x=0.043 m to x=0.108 m. **Tab. 1** summarizes thrust results under Condition 1 for different reconstruction methods. Two points are worth noting. First, for different methods, the close agreement in reconstructed pressure fields yields minimal thrust discrepancies (<0.5%). Second, for a given reconstruction method, both two thrust-computation approaches generate consistent results, as exemplified by the FVS method which exhibits relative errors of 0.50%. This reaffirms the high self-consistency of multi-physics parameters within the control volume, satisfying momentum conservation.

To sum up, given the absence of direct measurements, reconstructed data rationality can only be assessed indirectly through other related parameters or self-consistency verification. Two evaluation criteria for the PIV-based load measurement technology are summarized as follow. Criterion I is via wall pressure measurements, considering the reliable full-field pressures are unavailable. High-accuracy pressure serves as the foundation for load measurements. Criterion II assesses physical consistency via laws of mass and momentum conservation. If the mass flow rates and impulses derived totally by the PIV velocity data and the reconstructed data adhere to physical laws within defined tolerance thresholds, the results are deemed "self-consistent". Given error propagation, a 5% tolerance threshold is established. Criterion II is a necessary but insufficient condition, and thus it can assist in identifying unreasonableness and low fidelity but cannot serve as direct validation evidence. Conversely, criterion I constitutes the more critical and prioritized accuracy assessment standard.

Based on above criteria, for the through-flow condition of SERN, all three methods possess high pressure accuracy and good data consistency to obtain thrust, indicating the feasibility and reliability of PIV-based load measurement for nozzles.

Reconstruction methods	FVS method	Poisson method	SI method
Axial inlet impulse /(kg m s <sup>-2</sup> )	2837.58	2849.65	2858.31
Axial outlet impulse /(kg m s <sup>-2</sup> )	3075.73	3096.66	3124.15
Axial wall force /N	-222.80	-235.59	-216.91
Thrust <i>Th</i> ₁/N	3075.73	3096.66	3124.15
Thrust Th₂/N	3060.38	3085.24	3075.22
relative error E <sub>7</sub> (%)	0.50	0.37	1.59
Normal inlet impulse /(kg m s <sup>-2</sup> )	643.54	650.04	651.35
Normal outlet impulse /(kg m s <sup>-2</sup> )	950.03	960.18	967.79
Normal wall force /N	-340.77	-307.20	-353.63
Lift ∠ <sub>1</sub> /N	950.03	960.18	967.79
Lift L <sub>2</sub> /N	984.31	957.24	1004.98
relative error $E_{\ell}(\%)$	-3.48	0.31	-3.70

Table 1. Reconstructed thrust by different methods (case 1 of SERN)

#### 4.2. Case 2 of SERN

Fig. 10 presents the velocity field of SERN under Case 2 conditions (pw = 10174 Pa). The rising back pressure induces an oblique shock along the upper wall to achieve pressure balance, accompanied by a flow separation downstream. Limited by the FOV, only the separation point and minor separation bubble are captured. This condition simulates the over-expanded state with open separation. Fig. 11 shows the contours of the velocity component contours.

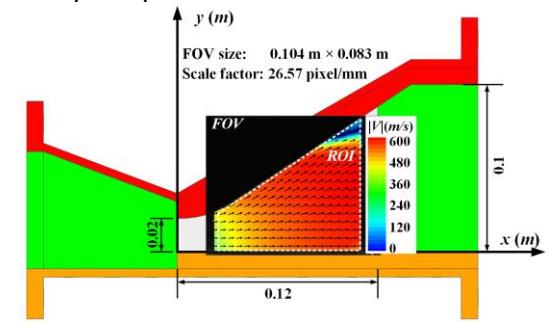


Fig 10. Contour of velocity field (case 2 of SERN)

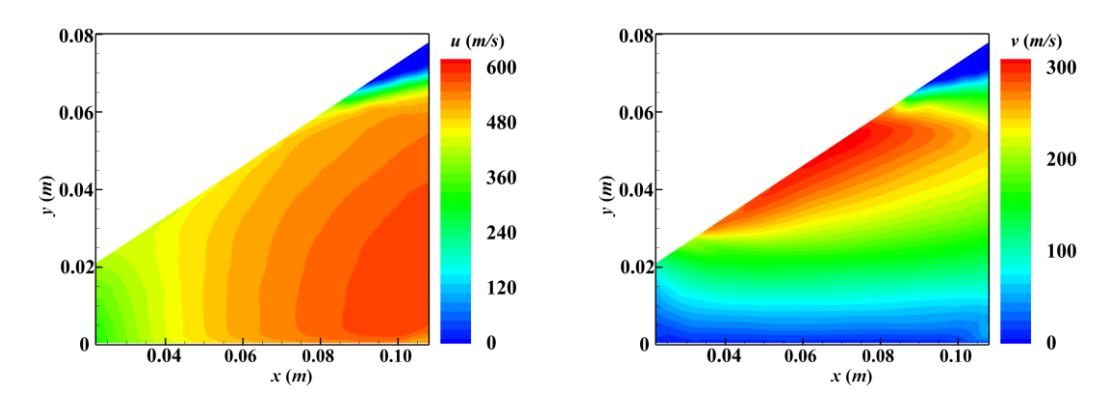


Fig 11. Contour of velocity component (case 2 of SERN)

Similarly, Fig. 12 presents the normalized reconstructed pressure field contours and the wall pressure distribution by different methods, respectively. The contours in Fig. 12(a)~(c) qualitatively provide a

global reference for pressure distribution. The upstream flow can be approximated as isentropic, and the reconstruction results are similar. However, significant differences emerge in the reconstruction accuracy among three methods once the shock arising. The performances of conventional Poisson and SI methods deteriorate to varying degrees, with relative errors reaching 26.9% and 74.3%, respectively. Although the Poisson result shows relatively smaller deviations, the positions and shapes of pressure contours do not match those of velocity contours around the shock. This is because the Poisson method employs an elliptic governing equation, which controls localized errors but also propagates errors upstream, causing the changes in flow structure near the shock. Conversely, the FVS method consistently maintains high accuracy, effectively propagating pressure information from upstream to downstream of the shock without causing error accumulation. **Fig. 12(d)** quantitatively reflects the above variation trends. These results demonstrate the feasibility and superior performance of the FVS method in supersonic flows with complex wave systems, indicating that the Steger-Warming flux vector splitting scheme and the upwind difference scheme can effectively handle mathematical discontinuities like shock.

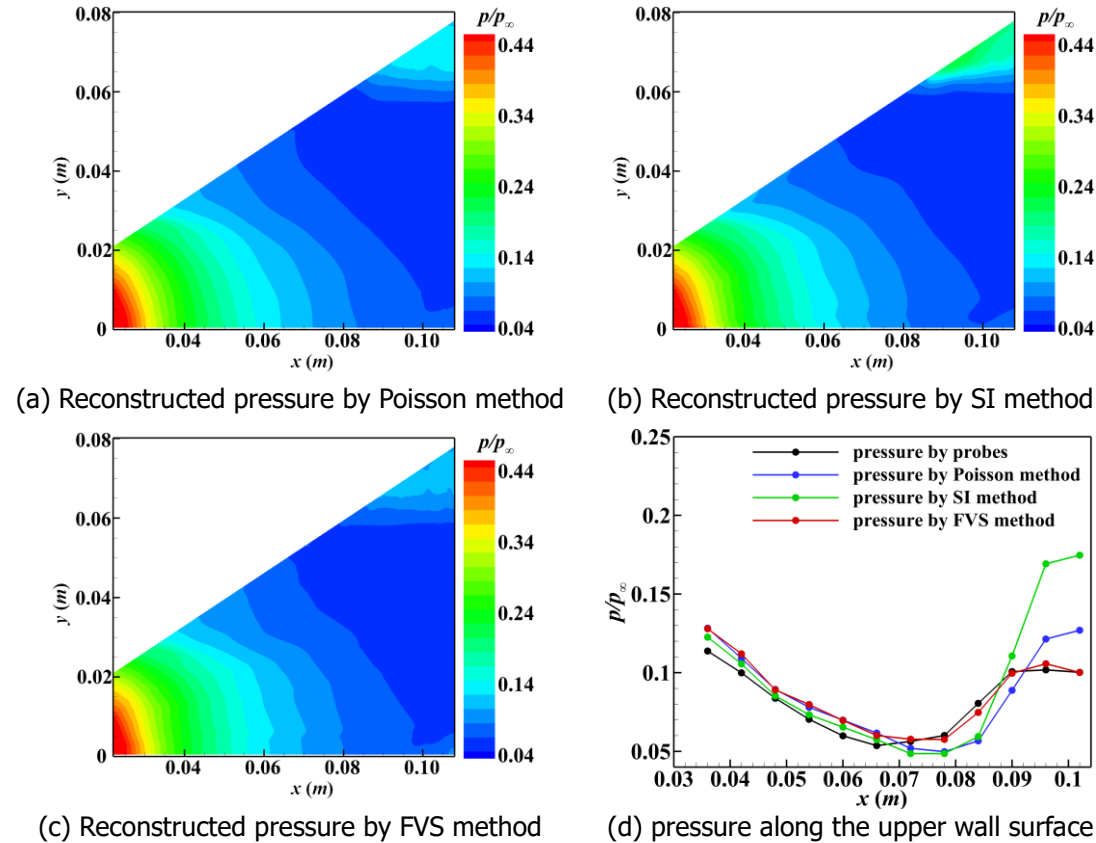


Fig 12. Reconstructed pressure results by different methods (case 2 of SERN)

With reference to the selection of control volume, the reconstructed mass flow rates at different cross-sections along the nozzle axis are monitored, as shown in **Fig. 13**. Upstream of the shock wave, the variation trend aligns with that of Case 1 and basically satisfies the law of mass conservation, with the evaluation results slightly higher than theoretical value. However, the amplitude of flow fluctuation has significantly increased downstream of the shock, deviating from mass conservation to varying degrees. This indicates the accuracy decrease of all three reconstruction methods. Specifically, the Poisson results are significantly overestimated, attributed to the error accumulation from excessively high static pressure estimates in the shear layer at the separation-mainstream interface. The SI results are underestimated due to its overestimation in the recirculation zone, especially the wall pressure. The FVS results exhibit relatively higher overall accuracy in pressure and mass flow.

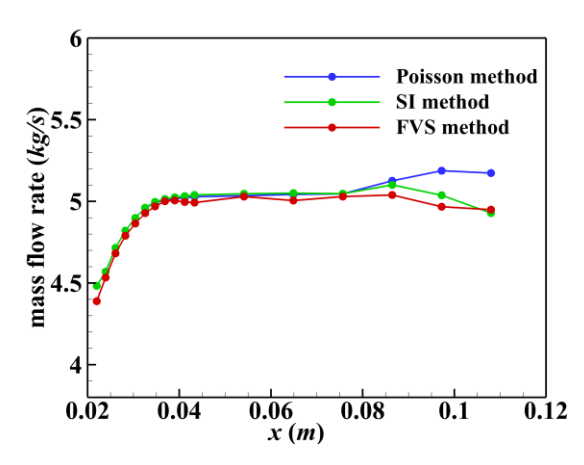


Fig 13. Reconstructed mass flow rate by different methods (case 2 of SERN)

The reconstructed thrust results for Case 2 are presented in **Tab. 2**. Similarly, nozzle thrust and lift are calculated by two mathematical formulations. The relative errors of FVS method between two formulations are -1.70% (thrust) and 0.60% (lift), respectively. This demonstrates good self-consistency of the multi-physics parameters, satisfying momentum conservation. In contrast, the Poisson and SI methods suffer from significantly deteriorated performance, and thus data self-consistency degraded and the accuracy decreases. The SI method, in particular, exhibits poor load reconstruction of nearly 30%. In summary, owing to the presence of complex flow structure with shock and separation region in case 2, the superiority of the FVS method exhibits more evidently relative to that in Case 1.

The synthesis of evaluations, including wall pressure, mass flow rate and aerodynamic loads, validates that the PIV-based reconstruction measurement is applicable to the internal flow of nozzles under over-expanded conditions and the FVS method exhibits superior performance to conventional methods.

Reconstruction methods	FVS method	Poisson method	SI method
Axial inlet impulse /(kg m s <sup>-2</sup> )	2849.21	2870.55	2877.43
Axial outlet impulse /(kg m s <sup>-2</sup> )	3145.42	3327.48	3233.58
Axial wall force /N	-350.64	-369.91	-476.43
Thrust <i>Th</i> ₁/N	3145.42	3327.48	3233.58
Thrust <i>Th</i> ₂/N	3199.85	3240.46	3353.86
relative error E <sub>7</sub> (%)	-1.70	2.69	-3.59
Normal inlet impulse /(kg m s <sup>-2</sup> )	631.52	630.96	629.15
Normal outlet impulse /(kg m s <sup>-2</sup> )	777.87	830.35	792.83
Normal wall force /N	-141.68	-148.62	19.67

777.87

773.20

0.60

830.35

779.58

6.51

**Table 2.** Reconstructed thrust and lift by different methods (case 2 of SERN)

#### 4.3. Case 1 of WTN

Lift L<sub>1</sub>/N

Lift L<sub>2</sub>/N

relative error E<sub>L</sub>(%)

As aforementioned, there were insufficient direct measurements to reliably evaluate the reconstruction results for the SERN model in this study, due to the absence of the flow meter and force balance. Furthermore, the high backpressure induced unsteady phenomena such as shock oscillations and flow separation, making it challenging to obtain high-accuracy RANS simulations consistent with the actual flow. Wall pressure measurements and data self-consistency were selected for evaluation, with the assessment criteria detailed in Section 4.1. Unlike the SERN, the WTN at its design point features isentropic expansion flow in the diffuser section and parallel, uniform flow within the diamond region—

HiSST-2025-357 Page | 12

792.83

609,48

30.08

both amenable to theoretical derivation. Therefore, numerical simulations and theoretical calculations provide more reliable references. This section comprehensively evaluates the reconstructed multiphysical fields, mass flow rates, and thrust loads using theoretical analytical solutions, RANS simulation results, and probe-based experimental measurements.

RANS simulations are performed using the experimental total temperature, total pressure, and backpressure as boundary conditions and the velocity field is shown in **Fig. 14(a)**. The nozzle's diamond region and FOV are marked. **Fig. 14(b)** presents the corresponding PIV data, showing general agreement with the simulation. However, two key observations warrant attention. First, a noise shock is induced by the interface between the lower metal wall and the optical window, compromising flow uniformity. Second, optical windows limit the effective FOV, preventing full coverage of the nozzle outlet section. Fortunately, this problem does not compromise reconstructed mass flow rate or thrust measurements as long as the control volume is appropriately selected.

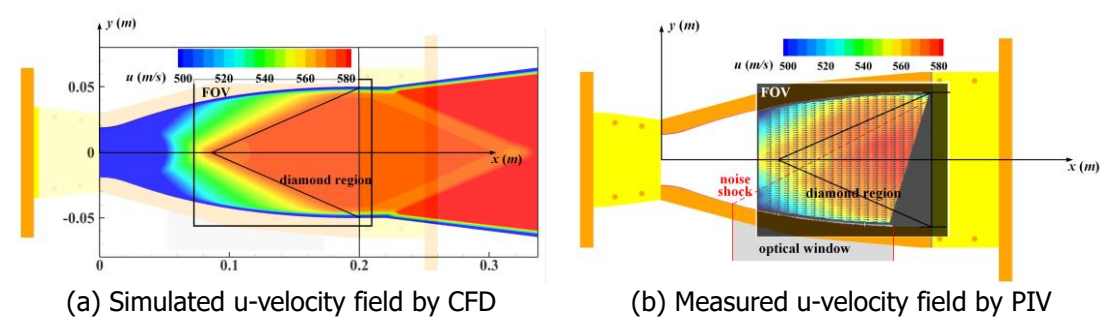


**Fig 14.** Contour of velocity field (case of WTN)

**Fig. 15** quantitatively illustrates the relative error distribution in the velocity field. The central FOV exhibited exceptional reconstruction accuracy, with errors below 1% except near the walls. Upstream regions maintained errors mostly within 2%, though noise-induced shock systems caused significant local deviations. Combined with wall reflections and optical distortion near the FOV boundaries, localized errors reached up to 4%. Overall, the velocity field measurements demonstrated good accuracy, validating the use of theoretical and simulated solutions for assessment.

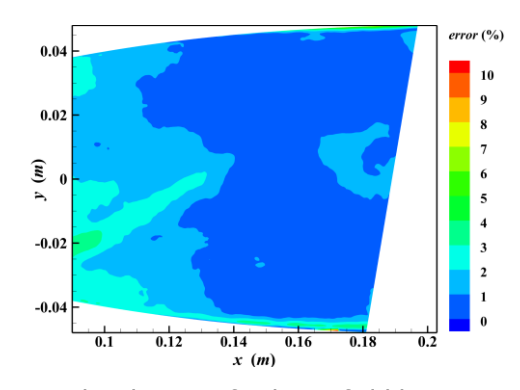
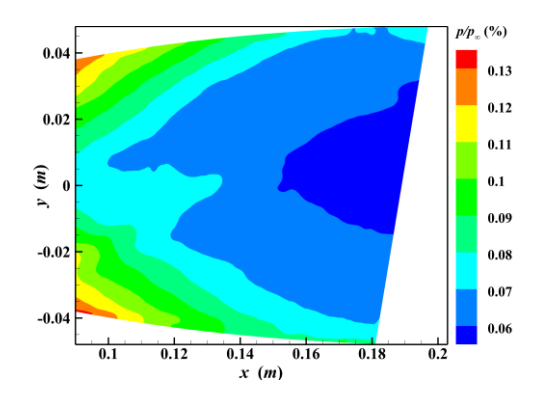


Fig 15. Contour of relative error distribution of velocity field between CFD and PIV (case of WTN)

**Fig. 16** shows the reconstructed pressure field. Given that two SERN cases have already demonstrated the feasibility and superiority of the FVS method—where conventional methods showed significant performance degradation—only the FVS method is further evaluated for the WTN model. The whole field exhibits smooth and continuous contours, except for localized concavity induced by noise shock slightly disrupting flow symmetry. **Fig. 17** compares the upper wall pressure distributions. the blue curve represents FVS-reconstructed pressure, while red and black curves denote RANS simulations and probe measurements, respectively. The FVS results slightly over-predict the wall pressure both upstream and downstream. In detail, upstream discrepancies arise from error propagation owing to the FOV's unavailability to capture near wall velocity data, yet accuracy remains within 3%. While

downstream discrepancies stem from interference by noise shock, causing slight flow deflection at nozzle outlet and generating additional noise-induced reflected shock structures in the downstream constant-area section. The simulations fail to capture this perturbations, while the probe measurements agree with the reconstruction. The results confirm that both probe-based pressure measurements and PIV-based velocity measurements accurately reflect the true flow structures and can mutually validate each other. In summary, the wall pressure distribution assessment validates the high accuracy of the FVS method and the feasibility of PIV-based reconstruction from two perspectives. It also indirectly verifies the correct aerodynamic contour design of the nozzle.



**Fig 16.** Reconstructed pressure field by FVS method (case of WTN)

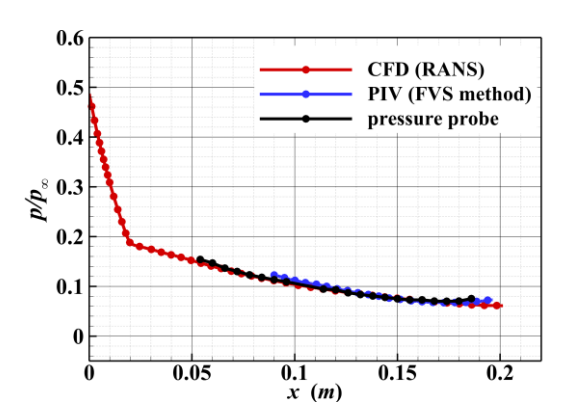
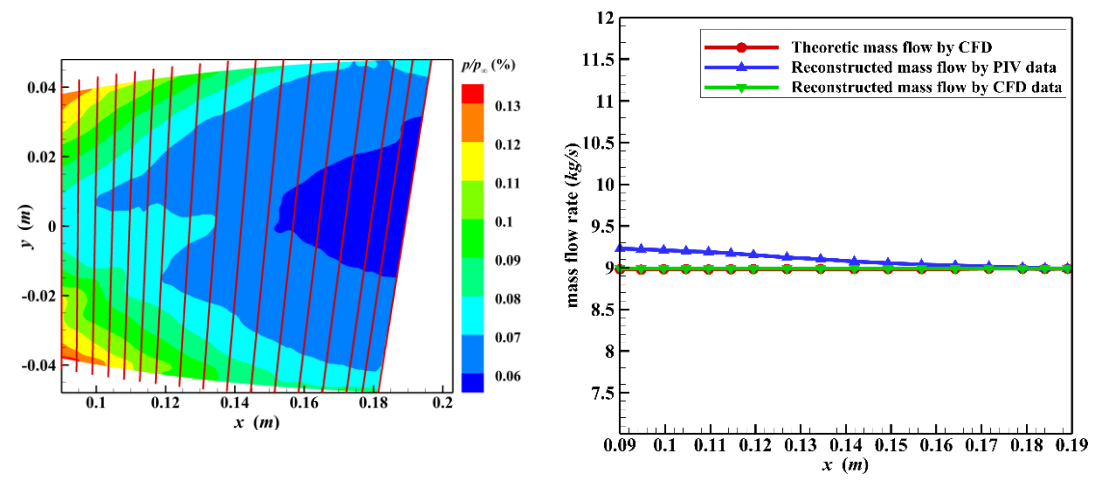


Fig 17. Comparative evaluation on reconstructed wall pressure by FVS method (case of WTN)

Subsequently, we evaluate the mass flow rate. Given that the effective FOV is asymmetric, inclined sections with progressively increasing slopes are used instead of vertical sections to extract the mass flow rate along the nozzle. The transfinite interpolation method under Lagrange-type functions is employed to determine the position of the monitor sections, shown in Fig. 18(a). In this way, the monitor sections can cover and examine the whole the effective FOV. In addition, each section is located using the x-coordinate of its center point. The reconstructed mass flow rates along different sections are compared with simulation results, shown in Fig. 18(b). The "CFD Theoretical Value by CFD" (red line) represents the mass flow rate directly extracted from the simulation data and the "Reconstructed Value by CFD" (green line) represents the mass flow rate obtained by applying the FVS reconstruction method to the CFD-simulated velocity field. Results show that the PIV-based reconstructed mass flow rate deviate only slightly from the theoretical value upstream, with errors controlled within an acceptable threshold range of less than 3%, and essentially satisfy mass conservation. Similar to pressure error distribution, upstream error primarily attributed to greater error propagation from velocity data. Conversely, downstream measurement accuracy, particularly near the walls, increases significantly, resulting in correspondingly higher reconstruction accuracy for the mass flow rate. This analysis further demonstrates the feasibility of mass flow reconstruction and highlights its dependence on measurement accuracy. Moreover, the mass flow rate reconstructed from the CFD-simulated velocity field using the FVS method agrees closely with the theoretical value, providing additional theoretical and quantitative validation of the FVS method's high accuracy.



(a) Inclined sections constructed along the axis (b) Mass flow rate extracted by different methods

Fig 18. Comparative evaluation on reconstructed mass flow rate by FVS method (case of WTN)

Finally, we evaluate the thrust reconstruction. The entire effective FOV is viewed as the control volume for thrust reconstruction, calculating both the momentum flux and wall force contributions. Tab. 3 evaluates the FVS reconstruction results against simulation results, listing the mass flow rate and momentum flux at the control volume inlet/outlet, along with the thrust results from two calculation approaches. Overall, all parameters except the axial wall force exhibit good reconstruction accuracy, with errors controlled within 3%. Specifically, mass flow rates have accurate results, consistent with the findings in **Fig. 18**. Momentum fluxes inherently robust against Gaussian random noise considering the calculation via surface integrals, and high reconstruction accuracy and precision is fully expected as long as the velocity field is reliable. As for the axial wall force, lower accuracy stems from several factors. Except for velocity error and noise shock, more important is that, both the reconstructed wall pressure errors and the elevated pressure zones concentrated upstream, which means that the pressures with larger errors conversely contribute more significantly to the load. These factors collectively amplify the error. However, despite the axial wall force error, thrust reconstruction maintains good overall accuracy. This is because the momentum flux contributes dominantly to the total thrust, while the axial wall force is negligible by comparison—typically differing by two orders of magnitude. Thus, errors in calculating the axial wall force have negligible impact on the overall accuracy of thrust reconstruction, and the reconstructed thrusts still maintain high accuracy with an error of 2.67%. The results of two calculation approaches are close, indicating the satisfaction of conservation of momentum

In conclusion, for the WTN at its design working condition, despite the presence of disturbances introduced by noise shock, the results still demonstrate that the non-intrusive PIV-based reconstruction method can simultaneously obtains a comprehensive set of parameters, including multi-physical fields, mass flow rate and thrust performance, and maintains good overall reconstruction accuracy within 3%. This validates the feasibility of the reconstruction measurement technology and the high performance of the optimized FVS method.

**Table 3.** Evaluations of Reconstructed aerodynamic loads and performance parameters by FVS method (case 1 of WTN)

	Theoretical value by CFD	Reconstructed value by PIV	relative error (%)
inlet mass /(kg s <sup>-1</sup> )	8.98	9.22	2.67%
outlet mass/(kg s <sup>-1</sup> )	8.98	8.99	0.11%
Axial inlet impulse /(kg m s <sup>-2</sup> )	5552.94	5662.80	1.98%
Axial outlet impulse /(kg m s <sup>-2</sup> )	5702.34	5721.54	0.34%
Axial wall force /N	162.12	204.76	26.30%
Thrust Th <sub>1</sub> /N	5702.34	5721.54	0.34%
Thrust Th <sub>2</sub> /N	5715.06	5867.56	2.67%

#### 5. Conclusion

This study proposes a supersonic pressure field reconstruction measurement method based on Flux Vector Splitting technique and applies it to PIV-based aerodynamic load measurements in supersonic nozzles. Through direct-connect PIV experiments, internal flow fields of a SERN model and WTN model under different conditions were simulated. Nozzle performance parameters including mass flow rate, thrust, and lift were indirectly measured based on reconstructed pressure fields. Key conclusions are as follows:

- (1) Feasibility of the PIV-based non-intrusive load measurement method is validated. Reconstructed multi-physical field parameters using the FVS method satisfy mass and momentum conservation laws. Wall pressure results align well with static pressure probe measurements. Thrust and lift measurements achieved relative errors of 0.50% and -3.84% for case 1 of SERN, and -1.70% and 0.60% for another, demonstrating excellent data self-consistency.
- (2) Superiority of FVS method is validated. The FVS-based pressure reconstruction method demonstrates feasibility and superiority in supersonic flows with complex shock wave, achieving local wall pressure reconstruction errors below 3% post-shock. In contrast, traditional Poisson and SI methods exhibit localized errors as high as 26.9% and 74.3%, respectively.

This work establishes a foundation for non-contact aerodynamic load measurement techniques in supersonic internal flows, offering new possibilities for high-accuray performance evaluation and mechanism analysis in complex propulsion systems.

#### References

- 1. Tropea, C., Yarin, A., Foss, J.F.: Springer Handbook of Experimental Fluid Mechanics. Springer, Berlin (2007) pp. 564–596
- 2. Rival, D.E., Van Oudheusden, B.W.: Load-estimation techniques for unsteady incompressible flows. Exp Fluids 58, 20 (2017)
- 3. Chen, K., Xu, J., Qin, Q., et al.: Modular design framework of an axisymmetric wrap-around thrust-optimized combined nozzle. Aerospace Science and Technology 127, 107690 (2022)
- 4. Jones, B.M.: The Measurement of Profile Drag by the Pitot-Traverse Method. HM Stationery Office, London (1936)
- 5. Raffel, M., Willert, C.E., Scarano, F., et al.: Particle Image Velocimetry: A Practical Guide (3rd edn.). Springer, Cham (2018) pp. 15–29
- 6. Adrian, R.J.: Twenty years of particle image velocimetry. Exp Fluids 39, 159–169 (2005)
- 7. Unal, M., Lin, J.C., Rockwell, D.: Force prediction by PIV imaging: a momentum-based approach. J Fluids Struct 11, 965–971 (1997)
- 8. Ragni, D., Van Oudheusden, B.W., Scarano, F.: Drag coefficient accuracy improvement by means of particle image velocimetry for a transonic NACA0012 airfoil. Meas Sci Technol 22(1), 017003 (2011)
- 9. Van Oudheusden, B.W., Scarano, F., Casimiri, E.W.F.: Non-intrusive load characterization of an airfoil using PIV. Exp Fluids 40, 988–992 (2006)
- 10. Van Oudheusden, B.W.: Principles and application of velocimetry-based planar pressure imaging in compressible flows with shocks. Exp Fluids 45, 657–674 (2008)
- 11. Van Oudheusden, B.W.: PIV-based pressure measurement. Meas Sci Technol 24, 390–392 (2013)
- 12. Zachos, P.K., Frascella, M., MacManus, D.G., et al.: Pressure flowfield and inlet flow distortion metrics reconstruction from velocity data. AIAA J 55(9), 2929–2941 (2017)
- 13. Liu, S., Xu, J., Yu, K.: MacCormack's technique-based pressure reconstruction approach for PIV data in compressible flows with shocks. Exp Fluids 58(6), 1–22 (2017)

- 14. Liu, S., Xu, J.: Assessment of pressure field and performance parameter reconstruction from velocity data for ramjet inlet. Aerosp Sci Technol 110, 106454 (2021)
- 15. Anderson, J.D.: Computational Fluid Dynamics: The Basics with Applications. McGraw-Hill, New York (1995) pp. 53–67
- 16. Steger, J.L., Warming, R.F.: Flux vector splitting of the inviscid gasdynamic equations with application to finite-difference methods. J Comput Phys 40(2), 263–293 (1981)
- 17. Van Leer, B.: Flux-vector splitting for the Euler equations. In: Lecture Notes in Physics, vol. 170, pp. 507–512. Springer, Berlin (1982)
- 18. Yu, K., Xu, J., Zhang, X., et al.: Inverse design of shock wave distortion for a direct-connect facility. Aerosp Sci Technol 55, 220–226 (2016)